Drought occurrence under future climate change scenarios in the Zard River basin, Iran

Pedram Mahdavi, Hossein Ghorbanizadeh Kharazi, Hossein Eslami, Narges Zohrabi and Majid Razaz

ABSTRACT

Global warming affected by human activities causes changes in the regime of rivers. Rivers are one of the most vital sources that supply fresh water. Therefore, management, planning, and proper use of rivers will be crucial for future climate change conditions. This study investigated the monitoring of hydrological drought in a future period to examine the impact of climate change on the discharging flow of the Zard River basin in Iran. Zard River is an important supplier of fresh and agricultural water in a vast area of Khuzestan province in Iran. A continuous rainfall-runoff model based on Soil Moisture Accounting (SMA) algorithm was applied to simulate the discharge flow under 10 scenarios (obtained from LARS-WG.6 software) of future climate change. Then, the Stream-flow Drought Index (SDI) and the Standard Precipitation Index (SPI) were calculated for each climate change scenario for the future period (2041–2060). The results of the meteorological drought assessment showed that near normal and moderate droughts had higher proportions among other drought conditions. Moreover, the hydrological drought assessment showed the occurrence of two new droughts (severe and extreme) conditions for the future period (2041–2060) that has never happened in the past (1997–2016).

Key words | climate change, continuous rainfall-runoff model, HEC-HMS, hydrological drought, hydrology

Pedram Mahdavi
Hossein Ghorbanizadeh Kharazi (corresponding author)
Hossein Eslami
Majid Razaz
Department of Civil Engineering-Water Resources Management, Shoushtar Branch,
Islamic Azad University,
Shoushtar,
Iran
E-mail: *ghorbanizadeh.iau@yahoo.com*

Narges Zohrabi
Department of Water Resources Engineering, Ahvaz Branch,
Islamic Azad University,
Ahvaz,
Iran

HIGHLIGHTS

- Examining two RCPs to evaluate runoff and precipitation in the future.
- Using of Soil Moisture Accounting (SMA) to compute excessive rainfall and rainfall-runoff modeling.
- Evaluating the interaction between SDI and SPI drought indices.
- Five AOGCMs under two RCPs were tested in the drought monitoring.
- Extreme droughts will occur in the future in this region and will decrease the water security.

INTRODUCTION

Drought and flood are two major events in Iran's climate. According to climatologists' points of view, the frequency and perpetuation of these events imply occurrence of climate change in Iran. Drought is a natural disaster which is not apparent until its final stage. In addition to precipitation patterns, other extreme climatic events such as severe temperature and low relative humidity often happen along with drought in many parts of the world, which can dramatically

doi: 10.2166/ws.2020.367

increase drought intensity. Drought is caused by a shortage of water in an area, leading to different effects in different parts, especially in the environment. Drought is not just a physical or natural phenomenon. The effect of drought on society is due to the interaction between a natural phenomenon (lower precipitation can be caused by natural climate change) and the people who need water. Therefore, the lack of attention to sustainable development in human activity, improper consumption and industrialized societies will exacerbate the effects of drought (Wilhite & Pulwarty 2017). Drought has been mainly studied in meteorological, hydrologic, agricultural and social-economical. In investigating meteorological drought, the frequency, duration, and intensity of low precipitation are studied. In the other studies, the effects of drought on rivers' discharge, changes in soil moisture and its human consequences are considered (Lioyd Hughes & Saunders 2002; Golian *et al.* 2015; Emadodin *et al.* 2019).

Two meteorological and hydrological droughts have been investigated in this paper. The hydrological drought occurs when the meteorological drought continues for a long time so that the rivers' flow or the underground water level decreases. This phenomenon occurs due to the lack of winter precipitation in the mid-latitudes (Yildiz 2009). Therefore, any change in the precipitation pattern can influence the amount and intensity of droughts. Many studies have been conducted on droughts. For example, Jasim & Awchi (2020) investigated regional meteorological drought in Iraq and employed the Standardized Precipitation Index (SPI). In this research, only the past period (1970–2013) was investigated. The results indicated that the mild drought has higher proportions among different types of meteorological droughts. Adib & Tavancheh (2018) investigated the relationship between drought indices using (SPI) and streamflow drought index (SDI) on Dez Watershed in Iran for the 1981–2012 period. They showed that the frequency and intensity of short-term droughts (with a 3-month scale) in some weather stations are higher than the frequency and intensity of long-term droughts (with 6, 9, and 12-month scales). Kubiak-Wójcicka & Bąk (2018) investigated the hydrological and meteorological drought and used SPI, Standardized Water-level Index (SWI) and Standardized Runoff Index (SRI) for the Vistula basin in Poland for the 1981–2010 period. It was determined that meteorological droughts occurred earlier in the northwestern and central part of the basin, and later in areas lying above 300 m a.s.l. (above sea level) and the south of Poland. Tabari *et al.* (2012) studied the hydrological drought in the northwest of Iran for the 1975–2009 period by applying SDI. Their results showed that almost all the stations suffered from extreme droughts during the study period. All the above studies either only use past periods to evaluate droughts or just use indices related to the precipitation. In this research, not only past and future periods are investigated, but also meteorological and hydrological droughts are considered. Consequently, these studies prove that drought monitoring by using different indexes is suitable to detect the duration and intensity of hydrological and meteorological droughts. Additionally, local managers and policy-makers can apply it to their water resources planning.

The fifth report of the Intergovernmental Panel on Climate Change (IPCC 2013) showed that global warming causes changes in the water cycle due to increases in concentrations of greenhouse gases. Moreover, the precipitation pattern will change more severely in dry and semi-dry areas of the world. Both flood occurrence and winter precipitation decrease can be the results of these changes. The climate change phenomenon influences the climate parameters and has negative effects on different systems of water resources, agriculture and environment. Different studies have been conducted on the climate change subject. For example, Maghsood *et al.* (2019) explored the climate change impact on flood frequency and source area in the northern part of Iran under Climate Model Intercomparison Project 5 (CMIP5) scenarios. To this end, they employed a median of the new CMIP5 General Circulation Models (GCMs) under Representative Concentration Pathways (RCP) scenarios (2.6 and 8.5). Besides, they used the SWAT model to generate future runoff. Their results revealed that the projected climate change would likely lead to an average discharge decrease in January, February, and March for both RCPs and an increase in September and October for RCP 8.5. Vu *et al.* (2017) assessed hydro-meteorological drought under climate change impact over the Vu Gia-Thu Bon river basin in Vietnam. In this research, only one emission scenario (A2) and three GCMs were used. The MIKE-SHE model was used to generate future runoff. The results suggest that, despite hotter and wetter future

climate, the area is likely to suffer more from severe and extreme droughts, increasing about 100% in the median range for drought characteristics. Different researchers use different GCMs and hydrological models to assess impact of climate change on droughts. In this study, continuous hydrological modeling using the HEC-HMS model was applied for the first time to simulate future runoff and assess the impact of climate change. Also, different GCMs under two emission scenarios (RCP45 and RCP85) are employed and investigated in depth.

These research studies imply that climate change, due to increasing Greenhouse Gases (GHGs), can have various effects on drought in different regions. Therefore, this research, as a case study, assesses the impacts of climate change on the hydrological drought of the Zard River basin, which is the only source to supply fresh water in a vast area. Its results will be very important for sustainable development. In this study, we used the new LARS-WG.6 downscaling software to derive 10 climate change scenarios from AOGCMs outputs for the future period (2041–2060). Then, we applied a soil moisture calculation algorithm to develop a continuous rainfall-runoff model simulating runoff discharge based on downscaled future climate conditions in the Zard River basin. The (SPI) and (SDI) are calculated under each climate change scenario to predict drought in the future period.

MATERIALS AND METHODS

Case study and data usage

Zard River is located in the east and northeast of Ramhormoz, southwest of Iran, within the geographic area of 49° 40′ to 50° 29′E longitude and 31° 05′ to 31° 42′ N latitude. The area of the basin is about 887 km^2. The map of this basin is shown in Figure 1.

Zard River is one of the main branches of ALAH River located in the Baghmalek (Janaki) area in Izeh (town), which has a very dense river network. The main and initial branch of this river is called Abul abbas or Bulavan. It originates from the eastern slopes of the Sefid Kuh and the Mongasht Mountain and flows toward the NW via narrow valleys in a mountainous area. Having crossed a valley with the same name in the Tang-e-Kure, it changes its direction toward the SW. This river, on its way, is the main water resource of villages such as Mal Agha, Robat-e-Abul Abbas, Zolab, and Sang. Later, and enters Baghmalek. This river joins Dom Ab Mangian, Ab Galal, Al-e-Khorshid, Dom Dali rivers and makes Zard River. Zard River, then flows toward the SW and supplies the main water source of villages such as Rud Zard Kafi, Rud Zard Sadat, Karim, and Jare. Near Rud Zard village, it joins Aala River and makes Alah River. Significant land uses in the study area are rangeland (48%), agriculture and urban areas (32%), woodland and forest (14%). Due to the importance of this basin the Jare dam was constructed on the Zard River in 2012. To monitor the drought, we used the data of two periods including the past period (1997–2016) and the future period (2041–2060). Meanwhile, 13 rain gauge stations were studied. Table 1 presents the stations by their characteristics. In Table 1, the historical period data (precipitation, runoff, temperature, and evaporation data) is provided by the Iran meteorological organization (a government agency) and the water utility company of Khuzestan province (a government agency). Also, soli map, land use-land cover and digital elevation maps were obtained from the water utility company of Khuzestan province.

The average annual precipitation in the studied drainage basin is about 580 mm and it varies from 402 to 792 among different stations. Table 2 shows the climate classification of Zard River basin based on the De Martonne method.

The basin's hydrology can be separated into wet and dry months. A substantially larger proportion of the annual flow is generated during the wet months. The wet (November to Jun) and dry (July to October) months flow account for about 85 and 15% of the total annual flows, respectively. Long-term monthly average flow (1987–2016) indicated that maximum and minimum runoffs occurred in April (15 m^3/s) and August (3.1 m^3/s), respectively.

Producing daily site-specific climate scenarios

The IPCC (2013) provides the most recent generation of GCMs in the fifth assessment report. The coupled models provide future projection simulations with specified concentrations referred to as 'representative concentration pathways' (RCPs), which are forced by anthropogenic

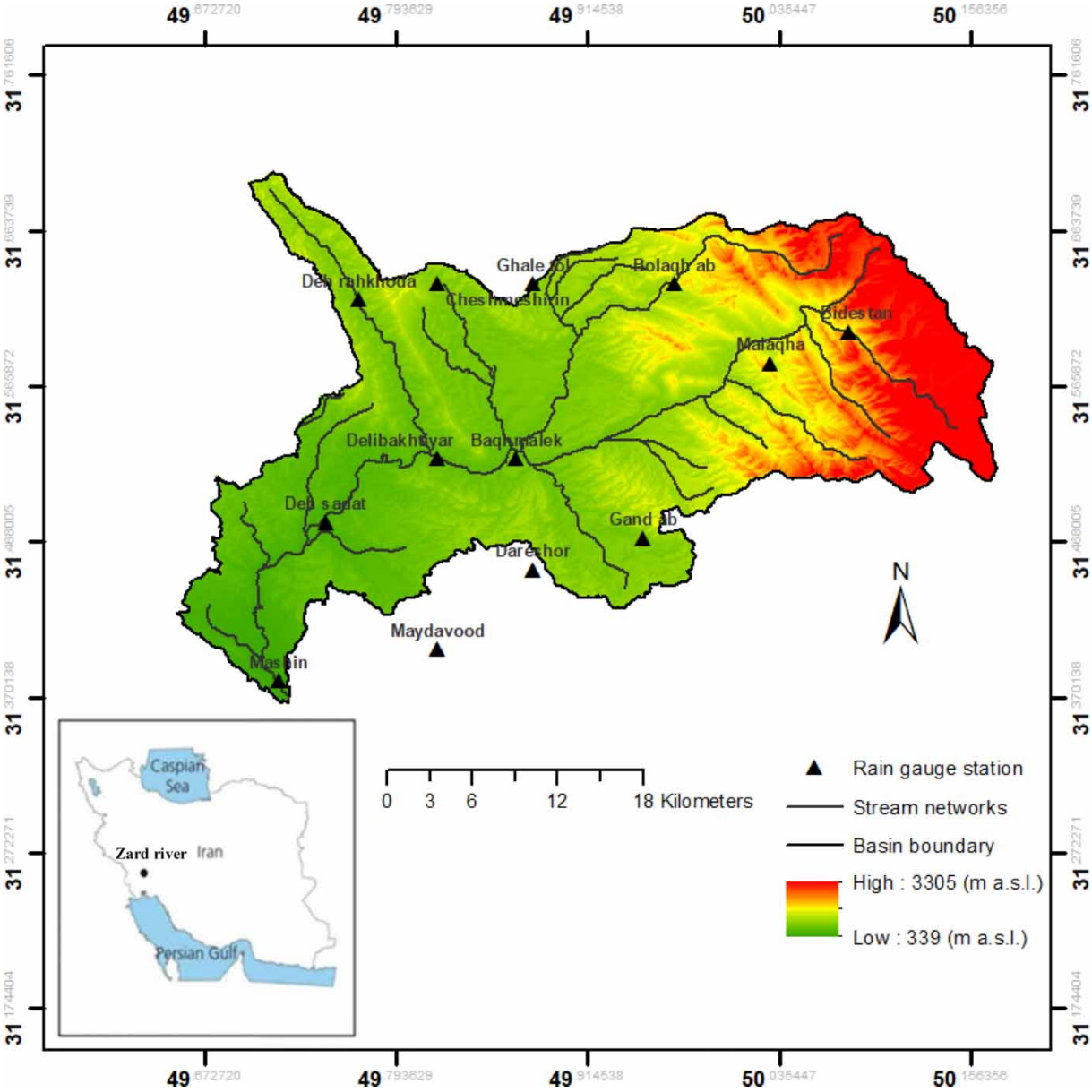

Figure 1 | The geographic map of Zard River drainage basin.

influences on the atmospheric composition and land cover (Taylor *et al.* 2011). The RCPs provide a roughly estimated range of the radiative forcing in the 21st century. The outputs of GCMs are presented in coarse resolutions because of our inability to model the Socio-Economic-Earth system. The need for accuracy in the climate change impact assessment models increases on finer spatial and temporal scales while the accuracy of GCMs, conversely, increases on finer scales. Hence, several methods have been widely developed for downscaling outputs of GCMs so that they can be used in impact studies (Chiew *et al.* 2010). In this research, we used downscaling outputs of 5 GCMs underlying RCP 45(as a balance condition) and RCP 85(as an extreme condition) from LARS-WG 6 software (Semenov *et al.* 1998) to produce climate change scenarios.

Table 1 | The characteristics of the rain gauge stations

Station name	Station type	Longitude (°E)	Latitude (°N)	Annual precipitation (mm) (1987–2016)		
				Min	Ave	Max
Bolagh ab	Rain gauge	49.58	31.33	345	708.7	1,235.5
Baghmalek	Rain gauge and evaporation poll	49.52	31.33	339	604.9	1,050.7
Mashin	Rain gauge, evaporation poll, hydrometric	49.43	31.23	226.5	416.4	717.3
Delibakhtiar	Rain gauge and evaporation poll	49.56	31.40	258	508.1	988.2
Ghale tol	Rain gauge	49.51	31.38	312	597.5	1,076
Gand ab	Rain gauge	49.47	31.27	274	583.2	931.5
Bidestan	Rain gauge	50.58	31.37	390	720	980
Cheshmehshirin	Rain gauge	49.47	31.38	246	641.5	1,092.5
Dareshor	Rain gauge	49.46	31.37	344	612	988
Deh rahkhoda	Rain gauge	49.46	31.35	245	620	985
Deh sadat	Rain gauge	49.45	31.20	210	452.8	787
Malagha	Rain gauge	50.02	31.35	396	792.1	1,589.5
Maydavood	Rain gauge	49.49	31.32	176	401.6	728.5

Table 2 | Climate classification of Zard River basin based on De Martonne method

Average annual precipitation (mm)	Average annual temperature (c°)	Aridity index	Climate
580	23.3	17.41	Semi-arid

LARS-WG 6 includes climate scenarios based on 5 GCMs. Table 3 shows the list of GCMs in the LARS-WG 6. It covers the whole period of 2041–2060 studied in this research. Also, Figure 2 shows the whole process of producing daily site-specific climate scenarios.

Drought indices

Drought indices are derived from short-term data series of precipitation, runoff, soil moisture, and river flows, in order to present an understandable large sample. To make better use of raw data to be understandable and increase the decision-making ability of designers and planners, we expressed the aforementioned indicators only numerically. We can use the obtained data of these indicators to detect the features of drought including duration, severity, and frequency. None of these indicators are superior compared to the other indicators, but some of them are more suitable for some applications (Barua *et al.* 2011). In this study, the

Table 3 | Characterization of climate models in LARS-WG6

Model name	Country	Institute
EC-EARTH	Netherlands/ Ireland	Irish Center for High-End Computing
GFDL-CM3	United States	Geophysical Fluid Dynamics Laboratory Industrial
HADGEM2-ES	Brazil	National Institute for Space Research
MIROC5	Japan	Atmosphere and Ocean Research Institute (The University of Tokyo), National Institute for Environmental Studies, and Japan Agency for Marine-Earth Science and Technology
MPI-ESM-MR	Germany	Max Planck Institute for Meteorology

Standardized Precipitation Index (SPI) and Streamflow Drought Index (SDI) were used in the interpretation of the meteorological and hydrological drought.

SPI index

This index is based on calculating the probability of rainfall for any timescale. SPI uses the monthly precipitation

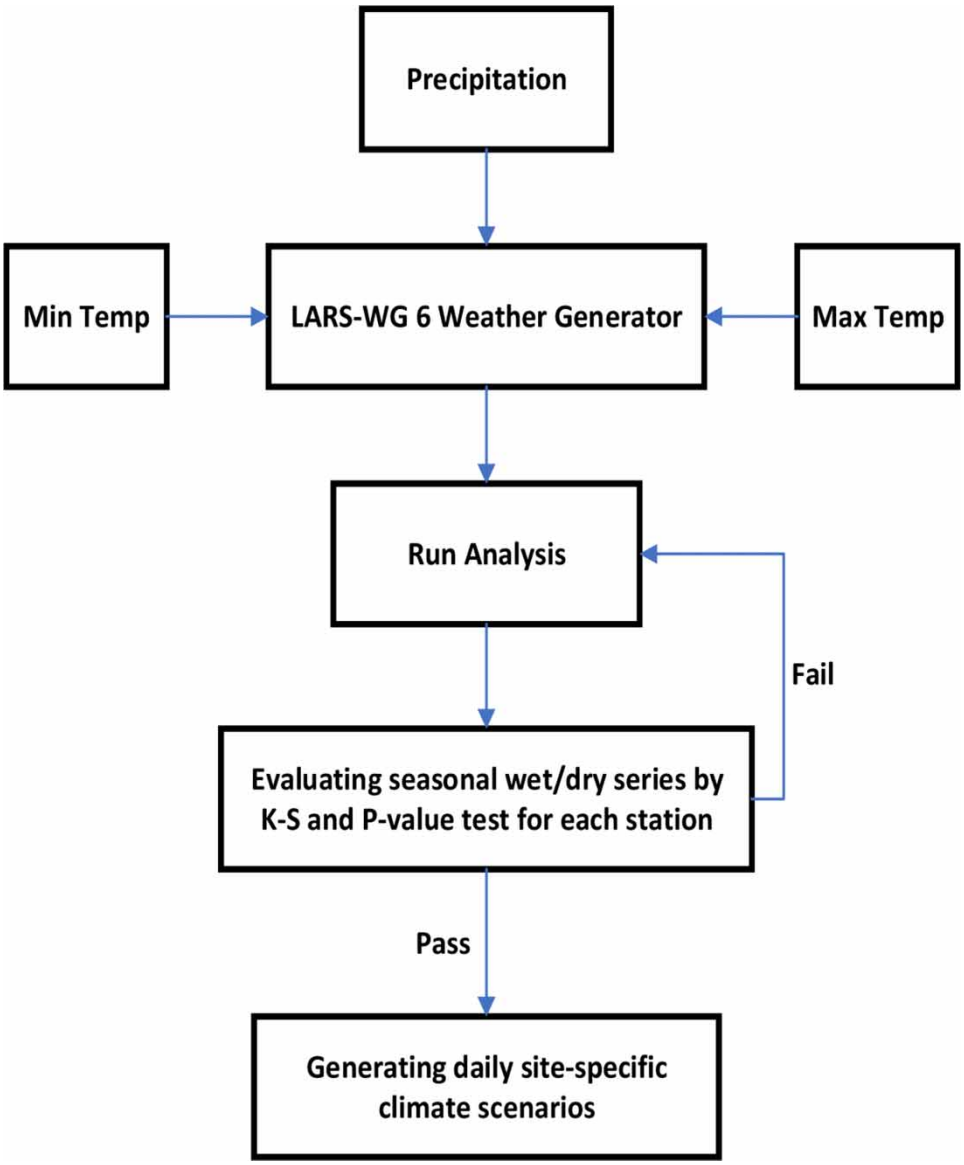

Figure 2 | Schematic of producing daily site-specific climate scenarios.

data to distinguish the shortage of rainfall at different time scales (3, 6, 12, 24 and 48 months). The first step in the calculation of standard precipitation is the fitness of standard gamma probability density function of the distribution of rainfall for a specific station (McKee *et al.* 1993). After calculating the total cumulative probability, we computed the standard normal random variable value, which shows similar probability to the mentioned probability that has zero mean and one standard deviation. The probability function is:

$$f(x;\alpha,\beta) = \frac{1}{\beta^{\alpha}\Gamma(\alpha)} x^{\alpha-1} e^{\frac{-x}{\beta}} \quad (1)$$

where α and β represent shape and scale, respectively, x represents the amount of precipitation and $\Gamma(\alpha)$ is the gamma function. We used the maximum likelihood

method to estimate the parameters α and β.

$$\hat{\alpha} = \frac{1}{4A}\left[1 + \sqrt{1 + \frac{4A}{3}}\right] \quad (2)$$

$$\hat{\beta} = \frac{\bar{x}}{\hat{\alpha}} \quad (3)$$

$$A = \ln(\bar{x}) - \frac{\Sigma \ln(x)}{n} \quad (4)$$

$\bar{x}$ is the average of precipitation and n is the number of days with observed rainfall. Gamma function is undefined for the precipitation number of zero ($x = 0$) since it is possible to have precipitation data equals to zero among the data. Therefore, the cumulative probability function that includes zero values is defined as follows:

$$H(x) = q + (1 - q).G(X) \quad (5)$$

where q is the zero chance of precipitation. If m is the number of precipitations, whose magnitude in the series equals zero, so q can be estimated from the $q = m/n$ equation. Changing the shape of the gamma cumulative probability is based on a random variable of Z (standard precipitation) with zero mean and variance. For a given month and time scale, the cumulative probability $G(X)$ of an observed amount of precipitation is given by:

$$G(X) = \frac{1}{\beta^{\alpha}\Gamma(\alpha)}\int_0^X x^{\alpha} e^{\frac{-x}{\beta}} \quad (6)$$

The drought happens when the amount of standard precipitation is continuously negative and becomes -1 or less, whereas positive values represent the termination of drought (Table 4). We can use the total negative values to analyze the characteristics of a standard rainfall drought (duration, magnitude, and intensity).

SDI index

To compute the SDI index, we used the equation below to make a data series from the mean of the monthly river discharge series (Qij) (Liu *et al.* 2012):

$$V_{i,k} = \sum_{j=1}^{3k} Q_{i,j} \quad i = 1,\ 2,\ \ldots$$
$$j = 1,\ 2,\ \ldots,\ 12 \qquad k = 1,\ 2,\ 3,\ 4 \quad (7)$$

where $V_{i,k}$ is cumulative flow discharge. In addition, i and j represent water year and the months of the water year, respectively. For example, If $k = 1$, $V_{i,k}$ is related to the first three months of water year for the i[th] water year. SDI based on these data sets of river flows and for the water year base period of k related to the i^{th} water year, SDI can be obtained from the following equation:

$$SDI_{i,k} = \frac{V_{i,k} - \bar{v}_k}{S_k} \quad (8)$$

$\bar{v}_k$ and S_k are the mean total volume flow rate and standard deviation of cumulative flow volume, respectively, for the base period k in a long time. Table 5 shows different drought states in the SDI method (Nalbantis 2008).

Table 4 | The drought classification based on the SPI

Wet or drought severity	Index value
Extremely wet	SPI $\geq +2$
Severely wet	$+1.99 \geq$ SPI $\geq +1.5$
Moderately wet	$+1.49 \geq$ SPI $\geq +1$
Near normal	$+0.99 \geq$ SPI ≥ -0.99
Moderate drought	$-1 \geq$ SPI ≥ -1.49
Severe drought	$-1.5 \geq$ SPI ≥ -1.99
Extreme drought	SPI ≤ -2

Table 5 | Classification of hydrological drought states, using the SDI index

State	Drought condition	Range	Percentage of probability
0	No drought	SDI ≥ 0	50
1	Mild drought	$0 >$ SDI ≥ -1	34.1
2	Moderate drought	$-1 >$ SDI ≥ -1.5	9.2
3	Severe drought	$-1.5 >$ SDI ≥ -2	4.4
4	Extreme drought	SDI < -2	3.3

Continuous hydrological modeling

The components of the continuous hydrological model used in this study are based on the HEC-HMS model, proposed by the Centre for Hydrology Engineering of the US Army Corps of Engineers. The modeling system is designed based on simulating rainfall-runoff models for a wide range of geographic locations and extensive issues (Feldman 2000; Roy *et al.* 2013; USACE-HEC 2015, 2016). The HEC-HMS model is made up of three main parts including: (1) the meteorological model (which contains methods used to describe precipitation and evaporation), (2) the basin model (including the methods to describe the physical characteristics of the river basin), and (3) control model (in which the starting and ending time of the stimulation is defined). The meteorological model and the basin model include different approaches to characterize physical and meteorological features of the basin by the user. For example, in the loss module, various ways exist depending on user interest for short-term (single event) or long-term modeling (continuous). Table 6 shows the calculation methods for all the components of the HEC-HMS model in this study.

This research employs continuous modeling based on the algorithm of Soil Moisture Accounting (SMA) to compute excessive rainfall, which is briefly explained as follows because of its importance. Some researchers (Gyawali & Watkins 2013; Koch & Bene 2013; De Silva *et al.* 2014; Khalid *et al.* 2016) showed an application of SMA to simulate rainfall-runoff in different regions.

Loss module

One of the most complex parts of hydrological modeling is the Loss module. This is because of a large number of activities that are computed simultaneously in the module; thus, the component values are required to be well defined. In this study, the algorithm of SMA was used. This algorithm is used to simulate the long-term relationship among precipitation, runoff, storage, evapotranspiration and soil loss in the basin. This algorithm divides the surface of the basin into five parts (Figure 3), which are separately explained below.

Since the formulas related to the algorithm of the soil moisture are unexplainable in their entirety in this research, only the main ones are discussed. These formulas include phenomena such as infiltration, percolation, lateral movement of groundwater, etc. The soil infiltration in the calculating algorithm of the soil moisture is computed by potential soil infiltration (PSI) (mm/hour), which is calculated by using the following equation (Bennett 1998):

$$PSI_t = MSI - \left(\frac{SOS_t}{SOS_m}\right) MSI \tag{9}$$

where MSI is the maximum infiltration of soil (mm/hour); SOS_t is the maximum capacity of the soil (mm) and SOS_m is the amount of water volume in the soil (mm). This

Table 6 | Calculation methods for components of the basin and meteorological models

Component	Calculation method
Canopy	Simple canopy
Surface	Simple surface
Loss	Soil moisture accounting
Transform	SCS unit hydrograph
Baseflow	Constant monthly
Evapotranspiration	Average monthly
Routing	Lag

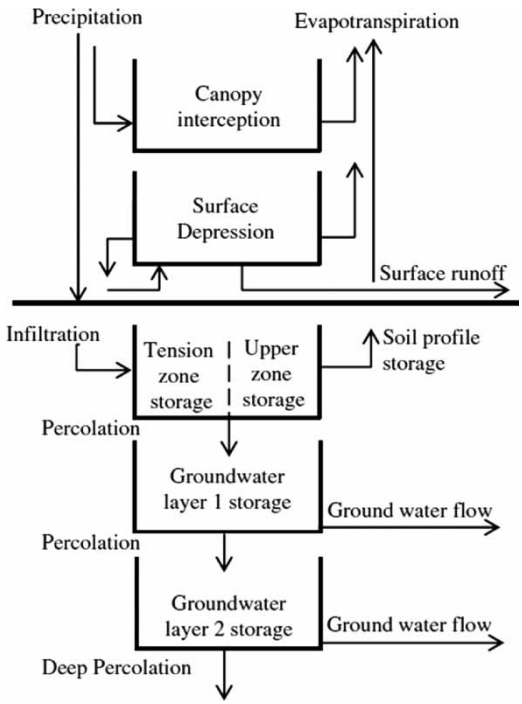

Figure 3 | Schematic view of continuous modeling, using the algorithm of SMA (De Silva *et al.* 2014).

equation implies that the potential soil infiltration cannot be more than maximum soil infiltration and it is linearly related to the water volume of the soil. If soil is without water or with a low amount of water, the potential soil infiltration can be equal to the maximum soil infiltration. Actual soil infiltration (ASI) at time t is calculated by the following equation:

$$ASI_t = min(PSI_t,\ AW_t) \tag{10}$$

where AW_t is the amount of permeable water. It is inferred from Equation (10) that actual soil infiltration cannot be more than current soil permeability. The percolation is similar to the permeability phenomenon, which is the water amount that reaches the groundwater via soil layers. Potential soil percolation (PSP) is calculated by the following equation (mm/hour):

$$PSP_t = MSP\left(\frac{SOS_t}{SOS_m}\right).\left(1 - \frac{GWS_t}{GWS_m}\right) \tag{11}$$

where MSP is the maximum soil percolation, SOS_t is the amount of water volume in the soil (mm), SOS_m is the capacity of the soil (mm), GWS_t is the storage of underground water for the current layer of water (mm) and GWS_m is the maximum storage of underground water (mm). Equation (11) shows that the potential soil percolation depends on the amount of water in the soil as well as the underground water. If the storage of underground water is in saturated or saturation condition, the large amount of water cannot permeate the groundwater aquifers. Actual soil percolation (ASP) is calculated similarly to Equation (10).

The output current of underground water layers indicates groundwater flow in a peripheral mode (a flow that is ultimately added as base flow to surface flow). The algorithm of soil moisture calculation of this peripheral current can be computed by the following equation:

$$GWF_{t+1} = \frac{(ASP_t) + GWS_t - (PGWP_t) - (0.5GWF_t.t)}{K + 0.5t} \tag{12}$$

GWF_t and GWF_{t+1} are the groundwater flow rates (mm) at the beginning of the time interval t and $t+1$, respectively; $PGWP_t$ is potential soil percolation of underground water (mm^3/hour); K is the coefficient of underground water storage layer(hour); t is the simulation time step.

Evaluating the hydrological model

For evaluating the model, we used the following equations:

Root Mean Square Error (RMSE) (Peak):

$$\text{RMSE} = \left[\frac{1}{n}\sum (Q_S - Q_O)\right]^{0.5} \tag{13}$$

Mean Absolute Error (MAE) (Peak):

$$\text{MAE} = \frac{1}{n}\sum_{i=1}^{n} |Q_S - Q_O| \tag{14}$$

Coefficient of Determination (R^2):

$$R^2 = \left[\frac{\sum (Q_O - \bar{Q}_O)(Q_S - \bar{Q}_S)}{\sqrt{\sum (Q_O - Q_O)^2 (Q_S - \bar{Q}_S)^2}}\right]^2 \tag{15}$$

Nash–Sutcliffe Efficiency (NSE):

$$\text{NSE} = 1 - \left\{\frac{\sum (Q_O - Q_S)^2}{\sum (Q_O - \bar{Q}_O)^2}\right\} \tag{16}$$

where Q_O, $\bar{Q}_O$ and Q_S are observed, averaged and simulated flows rates in m^3/s, respectively.

RESULTS

Rainfall-runoff modeling

We employed Continuous Hydrological Modeling to simulate future climate projections of runoffs and calibrated the continuous model of rainfall-runoff by using data of six water years (1975–76 to 1980–81). The water year in Iran is nearly from October to the end of September. For calibration and validation, we selected three: Baghmalek,

Ghale Tol, and Mashin stations, which represent the central part as well as the upper and lower elevations of the basin. Also, these three stations provided the required volume balance for simulation of runoff in the hydrometric station and showed a better correlation to each other relative to other stations. The discharge volume in Mashin hydrometric station represents the basin discharge volume. Fourteen parameters in the SMA loss model were calibrated. We estimated initial SMA parameters by employing the soil map, land use, land cover, and observed streamflow information. The model can be calibrated automatically and manually, both of which were applied in this study. Also, the model was calibrated and validated on a daily time scale. In the manual and automatic calibration, the RMSE was used as the objective function. Evaluation of the calibrated model was carried out by the Nash–Sutcliffe Efficiency (NSE), Root Mean Square Error (RMSE), Mean Absolute Error (MAE), Coefficient of Determination (R^2), as shown in Table 7. These results illustrate a close agreement between the simulated streamflow and observed flow. Also, Figure 4 shows that the model fitted very well in daily simulating the streamflow, base flows, and peak flows.

For validation of the model, the rainfall and runoff data of three water years (1998–1999 to 2000–2001) are used. Evaluation of the validated model is shown in Table 8. The results imply that there is a close agreement between the simulated streamflow and observed flow for the validation period. Figure 5 shows that the model can simulate daily runoff.

It is worth mentioning that the sensitivity parameter of the SMA algorithm was also performed. The sensitivity analysis of the SMA parameters helps to identify the effectiveness of model parameters or inputs (Wagener *et al.* 2009; O'Loughlin *et al.* 2013) and provides essential information about the model performance. The results show that the soil storage

Table 7 | Calibrated model evaluation

Water year	R^2 (Daily)	NSE (Daily)	RMSE (Daily) (m^3/s)	MAE (Daily) (m^3/s)
1975–76	0.797	0.796	11.1	4.2
1976–77	0.844	0.82	7.7	2.4
1977–78	0.757	0.66	8.6	2.9
1978–79	0.861	0.86	6.3	3.3
1979–80	0.761	0.667	9.1	3.9
1980–81	0.786	0.74	4.3	2.3
Overall	0.788	0.77	7.2	3.1

Table 8 | Validated model evaluation

Water year	R^2 (Daily)	NSE (Daily)	RMSE (Daily) (m^3/s)	MAE (Daily) (m^3/s)
1998–1999	0.78	0.776	4.2	2
1999–2000	0.764	0.65	4.6	2.2
2000–2001	0.791	0.727	5.5	2.1
Overall	0.772	0.72	4.4	2.1

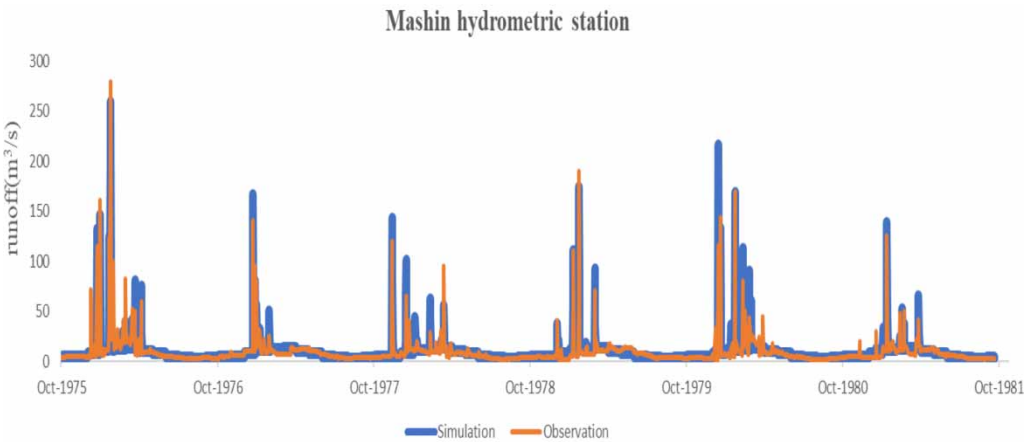

Figure 4 | Daily runoff in the calibration period.

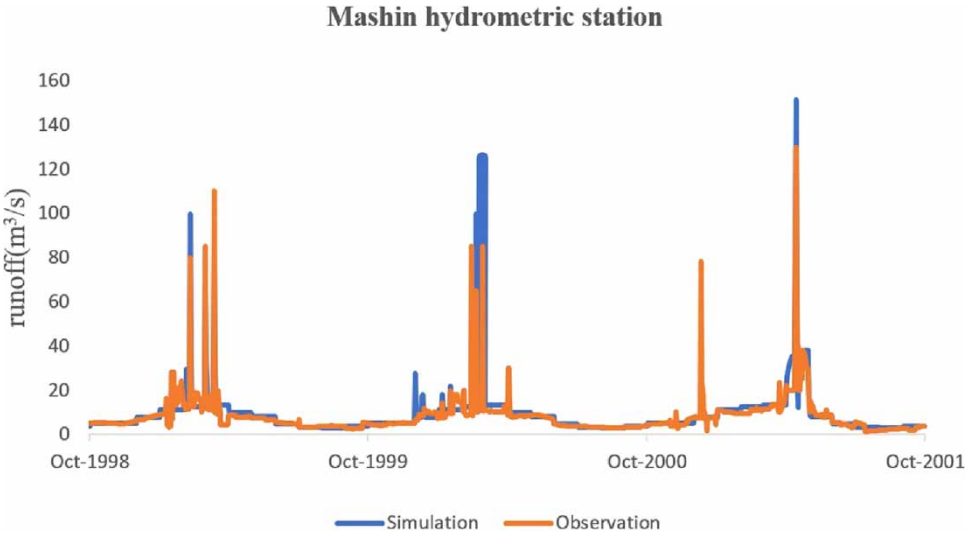

Figure 5 | Daily runoff in the validation period.

and tension storage are the most sensitive parameters, and groundwater 2 and groundwater 2 percolation are the least sensitive parameters in the loss module. Additionally, from sensitivity analysis, it can be concluded that the moisture condition of the upper soil layers affects sensitivity analysis more than the groundwater layers and this may be because of significant changes in the soil moisture conditions compared to the groundwater conditions. Also, it is worth mentioning that the baseflow method can also reduce the sensitivity of the groundwater parameters in some cases. The parameters' sensitivity ranking is presented in Table 9.

Table 9 | Sensitivity ranking of SMA parameters

SMA parameters	Sensitivity ranking	SMA parameters	Sensitivity ranking
Soil storage (mm)	1	Soil (%)	8
Tension storage (mm)	2	Groundwater 1(%)	9
Soil percolation (mm/hr)	3	GW1 percolation (mm/hr)	10
Max infiltration (mm/hr)	4	GW 2 storage (mm)	11
Impervious (%)	5	GW 2 coefficient (hr)	12
GW 1 storage (mm)	6	Groundwater 2 (%)	13
GW 1 coefficient (hr)	7	GW 2 percolation (mm/hr)	14

The meteorological drought and rainfall change

In this research, to assess annual meteorological drought, we calculated the SPI index for a 12-month interval for all selected rain gauge stations in both periods of the future and past. Figure 6 shows the temporal distribution of SPI based on 10 climate change scenarios in the future period compared to the baseline period. As is shown in Figure 6, near-normal had the highest rate among the five classification types and the results of different climate scenarios were similar. Meanwhile, the GFDL-CM3-RCP85 model showed the most near-normal condition and MIROC5-RCP45 showed the least near-normal condition. Moreover, the ECEARTH-RCP45 model presented the most extreme drought. The MIROC5-RCP85 and MIROC5-RCP45 models showed the most moderate drought and the EC-EARTH-RCP45 model showed the most severe drought. From a comparison of the previous and future periods, we can conclude that the extreme drought in the past period was higher (7–11%) than the future period. Besides, the severe and moderate droughts in the past period were usually lower than the future period. Changes in the near-normal condition vary in different models of the future period compared to the past period.

An investigation of the annual rainfalls shows that the precipitation increases in the future period compared to the past period. The models under the RCP85 scenario show more

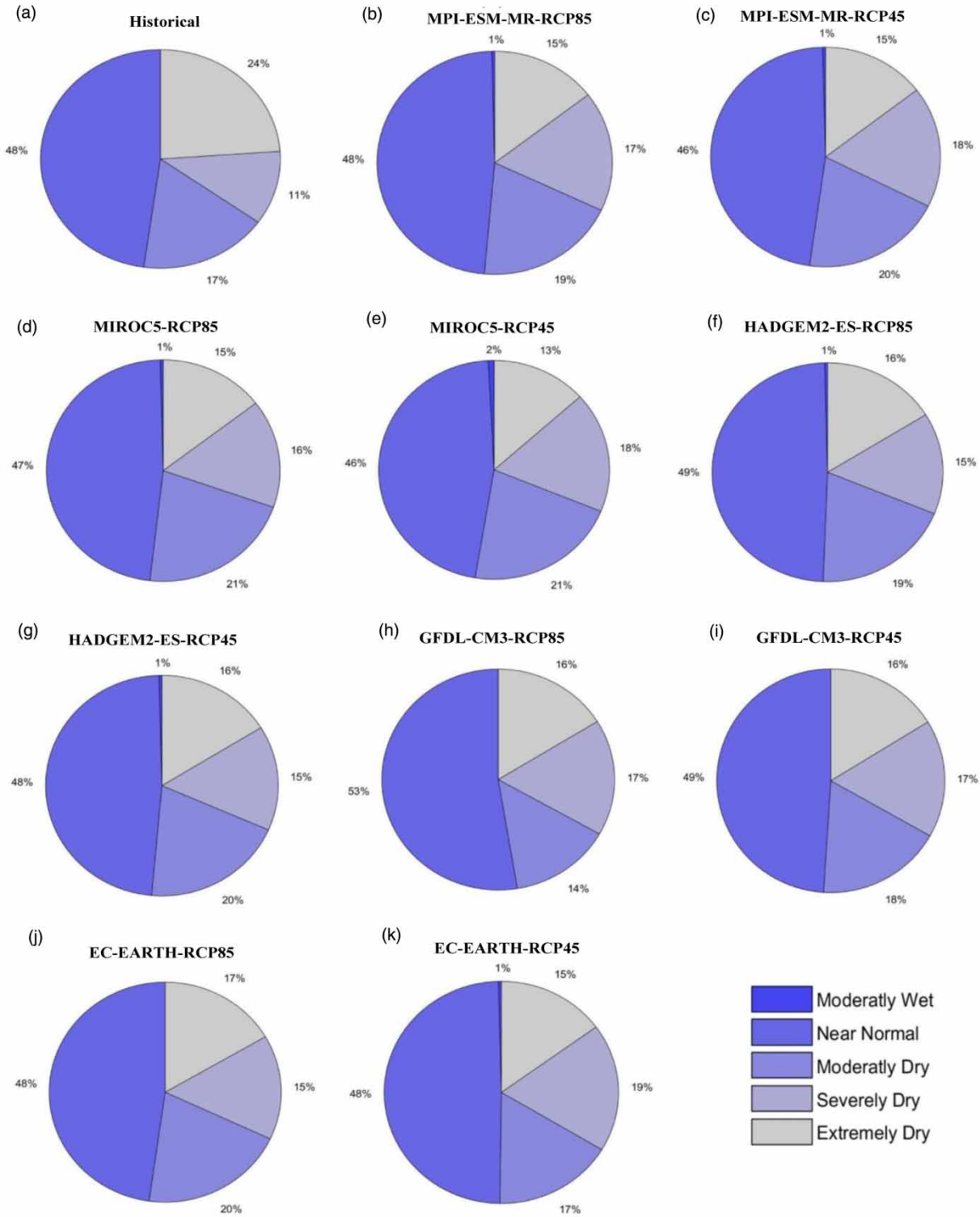

Figure 6 | Temporal distribution of SPI under climate change scenarios.

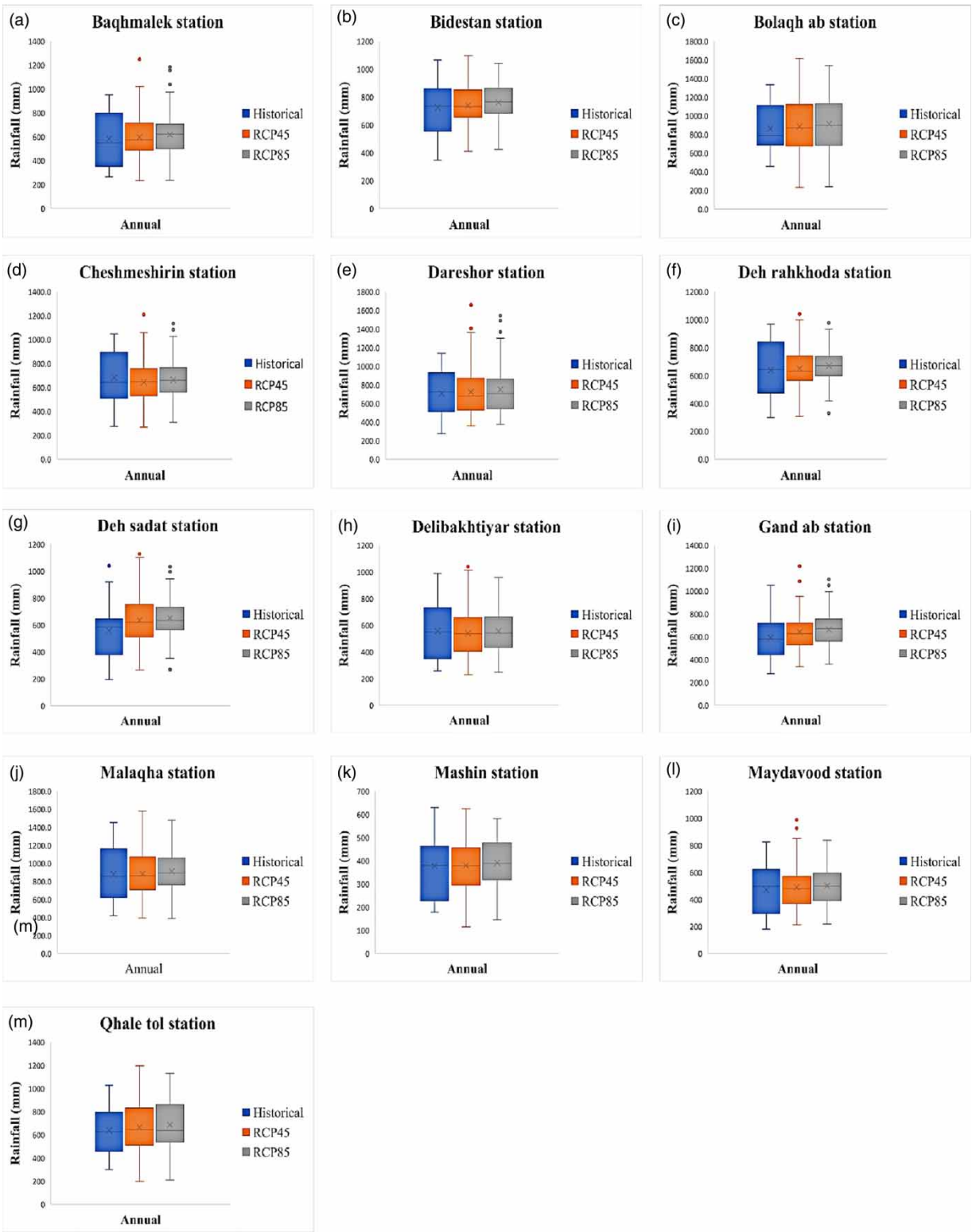

Figure 7 | Annual rainfall for historical (1997–2016) and future periods (2041–2060).

increase in precipitation compared to the models under the RCP45 scenario. The average precipitations under the RCP45 and RCP85 scenarios among all 13 stations increase to a maximum of 13.2 and 17%, respectively. Figure 7 shows the annual rainfall for all 13 stations. Overall, it can be concluded that the models under the RCP85 scenario show a more intensive change in precipitation compared to the models under the RCP45 scenario.

Hydrological drought index and runoff change

We evaluated the hydrologic drought using the SDI index. In order to evaluate the whole hydrological drought, we obtained and drew the index by using 10 climate scenarios for time intervals of 3, 6, 9, and 12 months in the period of 2041 to 2060 in the future and 1997 to 2016 in the past (Figures 8 and 9).

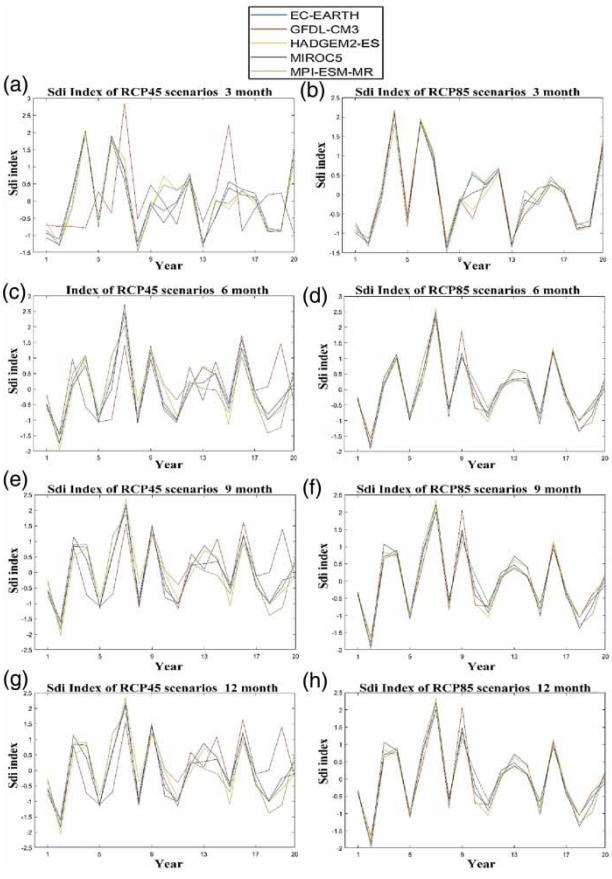

Figure 8 | SDI charts in the future period (2041–2060) for 3, 6, 9, 12-month intervals.

The biggest wet-state (no-drought) in 3, 6, 9, and 12-month time scales in the future is related to the GFDL-CM3-RCP45, MIROC5-RCP45, HADGEM2-RCP45, HADGEM2-RCP45 models respectively. The biggest severe drought in 6, 9, and 12-month time scales in the future is related to the HADGEM2-RCP45 model. The biggest wet-state in 3, 6, 9 and 12-month time scales in the past period is seen in years of 1999, 1997, 1997, and 1997, respectively. The biggest moderate drought in the past period in 3, 6, 9, and 12-month time scales is related to the year 2013. In general, contrary to the base period, severe drought will happen in the future that never happened before. Also, the RCP45 scenarios show more intensive droughts compared to the RCP85 scenarios. To clarify, we investigated the frequency of drought occurrence in the future. To do so, we calculated the occurrence percentage of each group of SDIs in the time scale of 3 to 12-months in the future and past periods, and presented them in Figures 10–12.

In the historical period, only mild and moderate droughts happened. But, in the future period, severe and extreme droughts will also happen. Moreover, the percentage of the occurrence of years without drought will be higher compared to the historical period. Thus, 4 to 9% will be added to the occurrence of years without droughts related to 3 to 12-month time scales. In the future, the percentage of the occurrence of drought will be decreased, but the type of drought will alter from moderate to severe. The mild droughts in the historical period will change from 40–55% to 35–43% in the future. The occurrence of moderate droughts in the future depending on the time scale of 3 to 12 months will be between 7–15%. The occurrence of the severe drought will increase from 0 in the historical period to 5% in the future period. The occurrence of extreme droughts in the future depending on the time scale of 3 to 12 months will be between 0–1%. Also, by increasing the time scale of 3 to 12 months, the fluctuation of occurrence of droughts will decrease; as, the occurrence of droughts of 9 and 12 months will be similar to each other. However, from the 3 to 6-month time scale, the difference in the percentage of occurrence of different types of drought and the no-drought conditions will be more obvious, which is related to the interannual fluctuations and changing of the seasons. It is obvious that the extreme condition of the RCP85 scenario caused more intense changes in drought

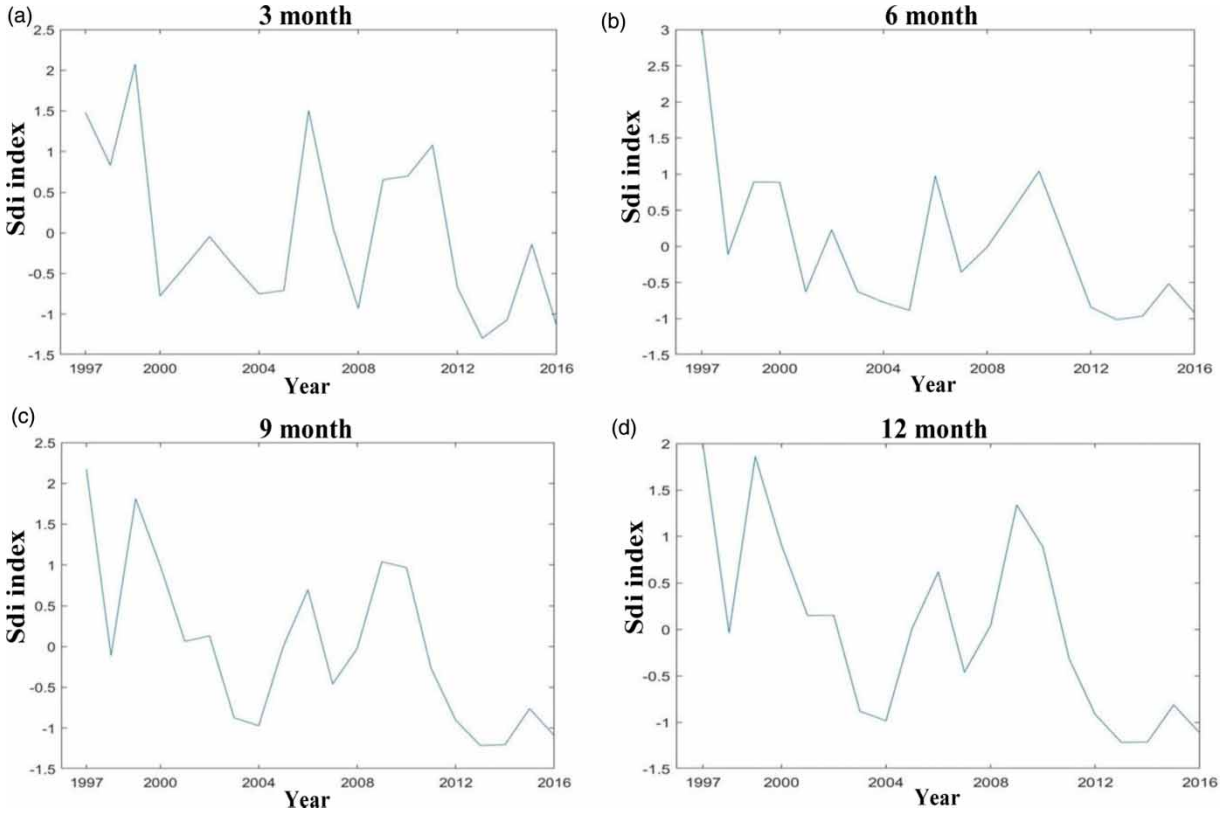

Figure 9 | SDI charts in the historical period (1997–2016) for 3, 6, 9, 12-month intervals.

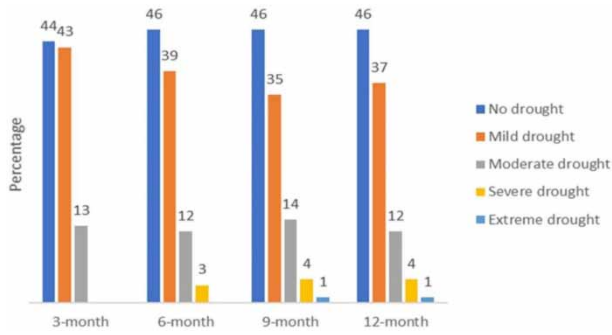

Figure 10 | Percent of occurrence of each group of 3 to 12-month SDI in the future period under RCP45 scenario.

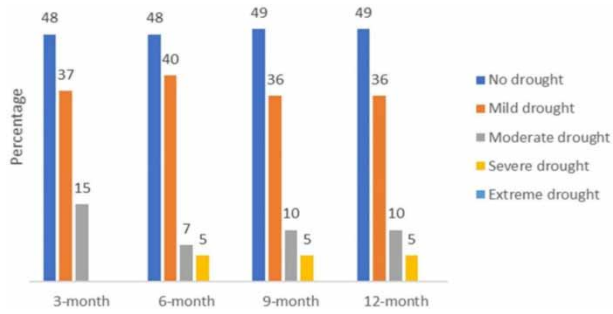

Figure 11 | Percent of occurrence of each group of 3 to 12-month SDI in the future period under RCP85 scenario.

conditions compared to the historical period as well as the RCP45 scenario.

Annual runoff analysis shows that the runoff will increase in the future compared to the historical period. Figure 13 shows the annual runoff for both future and historical periods. The results confirm that the models under the RCP85 scenario show more increase in runoff compared to the models under the RCP45 scenario. The runoff will increase by about 8.8 and 13% under the RCP45 and RCP85 scenarios respectively.

DISCUSSION

In this study, we used the new LARS-WG6 stochastic weather generator (one of the first studies or even the first study that

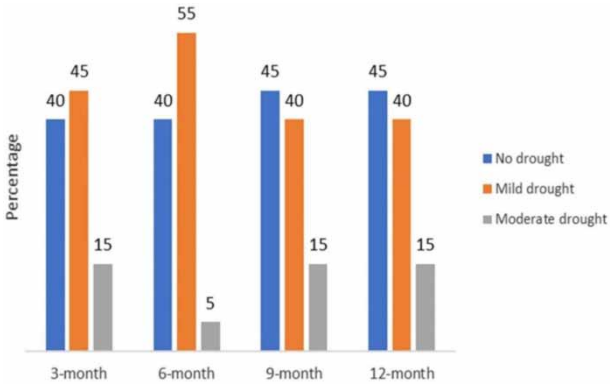

Figure 12 | Percent of occurrence of each group of 3 to 12-month SDI in the historical period.

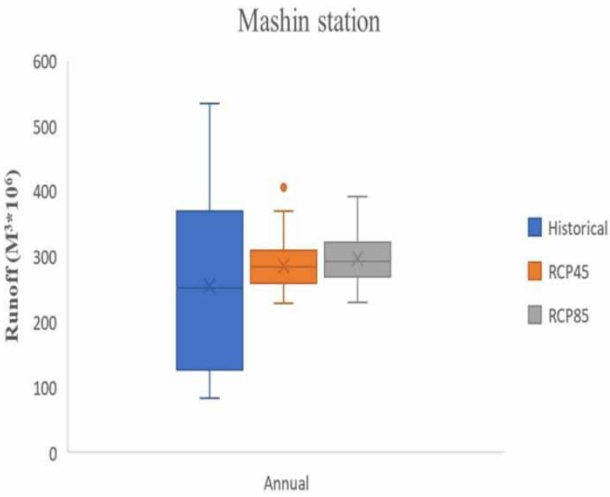

Figure 13 | Annual runoff for historical (1997–2016) and future (2041–2060) periods

uses the new version) to generate climate scenarios for impact assessments of climate change. Hence, this study can be a footstep for other researchers to evaluate and compare the outputs of this generator to other weather generators. Also, continuous hydrological modeling using SMA in the HEC-HMS model was used for the first time to project future runoff under climate change. The outputs showed an increase of average rainfall with a maximum of 13.2 and 17% under the RCP45 and RCP85 scenarios, respectively. Different studies confirm our results such as Chen *et al.* (2020). They investigated impacts of climate change and land use/land cover change on runoff in the Jinsha River Basin in China using SWAT model and 7 GCMs under RCP45 and RCP85 scenarios, respectively. They concluded that annual precipitation and run off will increase in the future by 9.26% and 14.66%, respectively. Our results confirm the increasing rainfall part of the Gebrechorko *et al.* (2019) research. In this study, they used only one GCM as an input for the SDSM and CanESM2 weather generators to project climate change scenarios. Also, Zheng *et al.* (2018), investigated future climate and runoff projections across South Asia from CMIP5 global climate models and hydrological modelling; their results indicated an increase in annual rainfall (11%) and annual runoff (maximum of 20%) that also confirms our projections. In this research, the H08 hydrological modeling was used to project future runoff. Nyaupane *et al.* (2018), predicted 43% increase of peak flows for the future period for Irwin Creek, Charlotte, North Carolina which confirms our results. In this study, the Hadley Center Coupled Global Climate Model (HRM3-HADCM3) and event-based method in the HEC-HMS model was used to predict peak flows in the future. The results of our study are inconsistent with Dongwoo's study (2018), in which the author concluded that the average rainfall would not change in the future under the RCP85 scenario (this scenario was only investigated in the study). Another study conducted by Bajracharya *et al.* (2018) showed an increase in precipitation and runoff under the RCP85 scenario which confirms our results. However, the increase in average runoff is much higher (50% increase in runoff) compared to our research (13% increase in runoff) and this is because of high snowmelt in the case study of the article.

In this research, the meteorological and hydrological droughts were estimated by SPI and SDI indices, respectively. The results of the meteorological droughts show that the extreme droughts decrease in the future period under both RCP45 and RCP85 scenarios compared to the past period. These results are inconsistent with the study of Ahmadebrahimpour *et al.* (2019). They concluded that extreme droughts would increase, especially under the RCP85 scenario. Meanwhile, severe and moderate droughts would increase in the future period compared to the past period, and this is in agreement with our research. The hydrological drought assessment in our study shows that no drought condition will increase (4–9%) in the future period compared to the historical period. Besides, mild droughts will occur more than other droughts. The future projections show more intense changes in drought conditions, which is consistent with the Bouabdelli *et al.*

(2020) research. They investigated hydrological drought risk recurrence under climate change in the karst area of Northwestern Algeria. The results illustrated that the risk of occurrence of more severe droughts in the future is higher than the past period. Vu *et al.* (2017) assessed hydro-meteorological drought under climate change impact over the Vu Gia-Thu Bon river basin in Vietnam. Their results indicated that more severe and extreme hydrological droughts will happen in the future compared to the past period, which confirms our results.

Most of the mentioned studies focused only on the prediction of droughts but they did not suggest or investigate any adaption strategies to tackle the impact of climate change on droughts. Consequently, we have summarized some of the popular adaption strategies below based on the previous research.

- Preserving water resources (Morid *et al.* 2012; Keshavarz *et al.* 2013; Moradi *et al.* 2013)
- Developing early warning systems and emergency response systems (Keshavarz *et al.* 2013)
- Extending efficient systems for water use (WAVA (2015))
- Providing relief funds for drought (Keshavarz *et al.* 2013)
- Enhancing and modernizing old irrigation facilities and canals (WAVA 2015)
- Boosting existing optimum cropping patterns (NRIDR 2005; Morid *et al.* 2012; Moradi *et al.* 2013)

It is important to mention that the outputs of this study only showed some potential change in meteorological and hydrological droughts. Different GCMs under different RCPs may generate different outputs. Also, SPI and SDI have some setbacks. The only inputs for these indices are rain and runoff.

CONCLUSIONS

The analysis of the SPI index showed that near-normal and moderate droughts have higher proportions among different types of meteorological droughts. A comparison between the historical period and future period indicates that the frequency and pattern of extreme drought will change in the future. These results can indicate that the future change in droughts can move outside the historical envelope due to climate change. An analysis of the SDI index showed that the number of droughts in the past period was more than the future period. However, the intensity of the drought is higher in the future period compared to the past period. These results can indicate that the RCP45 and RCP85 scenarios may cause higher temperature change and a warming atmosphere causes more evaporation. That is, more water is available for precipitation; thus, it may be the reason for more intense changes in drought conditions in the future period. Also, severe and extreme droughts will occur in the future period that have not happened in the past period. Based on the intensity of the occurrence of droughts in the future period, we recommend more investigations into adaptation strategies guidance for water supply and food production to meet severe droughts. Our suggestions for water resources managers to deal with the adverse effects of climate change are as follows:

- Extending efficient systems for water use
- Providing certain technologies for the proper management of farms
- Preserving the existing soil and ground water resources
- Utilizing popular media, including radio and TV, to manage education and awareness campaigns

FUNDING

This research received no external funding.

ACKNOWLEDGEMENTS

We would like to thank the Iran meteorological organization and water utility company of Khuzestan province for providing necessary data for this study.

CONFLICTS OF INTEREST

The authors declare no conflict of interest.

DATA AVAILABILITY STATEMENT

All relevant data are included in the paper or its Supplementary Information.

REFERENCES

Adib, A. & Tavancheh, F. 2018 Relationship between hydrologic and metrological droughts using the streamflow drought indices and standardized precipitation indices in the Dez Watershed of Iran. *International Journal of Civil Engineering* **17**, 1171–1181. doi:10.1007/s40999-018-0376-y.

Ahmadebrahimpour, E., Aminnejad, B. & Khalili, K. 2019 Assessing future drought conditions under a changing climate: a case study of the Lake Urmia Basin in Iran. *Water Supply* **19**, 1851–1861. doi:10.2166/ws.2019.062.

Bajracharya, A., Bajracharya, S., Shrestha, A. & Maharjan, S. 2018 Climate change impact assessment on the hydrological regime of the Kaligandaki Basin, Nepal. *Science of the Total Environment.* **625**, 837–848. doi:10.1016/j.scitotenv.2017.12.332.

Barua, S., Ng, A. W. M. & Perera, B. J. C. 2011 Comparative evaluation of drought indexes: case study on the Yarra River Catchment in Australia. *Journal of Water Resources Planning and Management – ASCE* **137**. doi:10.1061/(ASCE)WR.1943-5452.0000105.

Bennett, T. H. 1998 *Development and Application of A Continuous Soil Moisture Accounting Algorithm for the Hydrologic Engineering Center Hydrologic Modeling System (HEC-HMS)*. MS thesis. Dept. of Civil and Environmental Engineering, University of California, Davis, CA. doi:10.1061/40517(2000)149.

Bouabdelli, S., Meddi, M., Zeroual, A. & Alkama, R. 2020 Hydrological drought risk recurrence under climate change in the karst area of Northwestern Algeria. *Journal of Water and Climate Change* **11**, 164–188. doi:10.2166/wcc.2020.207.

Chen, Q., Chen, H., Zhang, J., Hou, Y., Shen, M., Chen, J. & Xu, C. 2020 Impacts of climate change and LULC change on runoff in the Jinsha River Basin. *Journal of Geographical Sciences* **30**, 85–102. doi:10.1007/s11442-020-1716-9.

Chiew, F. H. S., Kirono, D. G. C., Kent, D. M., Frost, A. J., Charles, S. P., Timbal, B., Nguyen, K. C. & Fu, G. 2010 Comparison of runoff modeled using rainfall from different downscaling methods for historical and future climates. *Journal of Hydrology* **387** (1–2), 10–23. doi:10.1016/j.jhydrol.2010.03.025.

De Silva, M. M. G. T., Weerakoon, S. B. & Herath, S. 2014 Modeling of event and continuous flow hydrographs with HEC–HMS: case study in the Kelani River Basin, Sri Lanka. *Journal of Hydrologic Engineering* **19** (4). doi:10.1061/(ASCE)HE.19435584.0000846, 800-806.

Dongwoo, J. 2018 Assessment of meteorological drought indices in Korea using RCP 8.5 scenario. *Water* **10**, 283. doi:10.3390/w10030283.

Emadodin, I., Reinsch, T. & Taube, F. 2019 Drought and desertification in Iran. *Hydrology* **6**, 66. doi:10.3390/hydrology6030066.

Feldman, A. D. 2000 *Hydrologic Modeling System HEC-HMS: Technical Reference Manual*. US Army Corps of Engineers, Davis, CA. Hydrologic Engineering Center.

Gebrechorko, S. H., Hülsmann, S. & Bernhofer, C. 2019 Regional climate projections for impact assessment studies in East Africa. *Environmental Research Letters* **14**, 044031. doi:10.1088/1748-9326/ab055a.

Golian, S., Mazdiyasni, O. & AghaKouchak, A. 2015 Trends in meteorological and agricultural droughts in Iran. *Theoretical and Applied Climatology* **119**, 679–688. doi:10.1007/s00704-014-1139-6.

Gyawali, R. & Watkins, D. W. 2013 Continuous hydrologic modeling of snow-affected watersheds in the Great Lakes basin using HEC-HMS. *Journal of Hydrologic Engineering* **18** (1), 29–39. doi:10.1061/(ASCE)HE.19435584.0000591.

IPCC 2013 Summary for Policymakers. In: *Climate Change 2013: The Physical Science Basis. Contribution of Working Group I to the Fifth Assessment Report of the Intergovernmental Panel on Climate Change* (T. F. Stocker, D. Qin, G.-K. Plattner, M. Tignor, S. K. Allen, J. Boschung, A. Nauels, Y. Xia, V. Bex & P. M. Midgley eds). Cambridge University Press, Cambridge, United Kingdom and New York, NY, USA.

Jasim, A. I. & Awchi, T. A. 2020 Regional meteorological drought assessment in Iraq. *Arabian Journal of Geosciences* **13**, 284. doi:10.1007/s12517-020-5234-y.

Keshavarz, M., Karami, E. & Vanclay, F. 2013 Social experience of drought in rural Iran. *Land Use Policy* **30**, 120–129.

Khalid, K., Ali, M. F., Rahman Abd, N. F. & Mispan, M. R. 2016 Application on one-at-a-time sensitivity analysis of semi-Distributed hydrological model in tropical watershed. *International Journal of Engineering and Technology* **8** (2), 132–136. doi:10.7763/IJET.2016.V8.872.

Koch, R. & Bene, K. 2013 Continuous hydrologic modeling with HMS in the Aggtelek Karst region. *Hydrology* **1** (1), 1–7. doi:10.11648/j.hyd.20130101.11.

Kubiak-Wójcicka, K. & Bąk, B. 2018 Monitoring of meteorological and hydrological droughts in the Vistula basin (Poland). *Environmental Monitoring and Assessment* **190** (11), 691. doi:10.1007/s10661-018-7058-8.

Lioyd Hughes, B. & Saunders, M. A. 2002 A drought climatology for Europe. *International Journal of Climatology.* **22**, 1571–1592. doi:10.1002/joc.846.

Liu, L., Hong, Y., Bednarczyk, C. N., Yong, B., Shafer, M. A., Riley, R. & Hocker, J. E. 2012 Hydro-climatological drought analyses and projections using meteorological and hydrological drought indices: a case study in Blue River Basin. Oklahoma. *Water Resources Management* **26**, 2761–2779. doi:10.1007/s11269-012-0044-y.

Maghsood, F. F., Moradi, H., Bavani, A. R., Panahi, M., Berndtsson, R. & Hashemi, H. 2019 Climate change impact on flood frequency and source area in northern Iran under CMIP5 scenarios. *Water* **11**, 22, 273. doi:10.3390/w11020273.

McKee, T. B., Doesken, N. J. & Kleist, J. 1993 The Relationship of Drought Frequency and Duration to Time Scales. In: *Proceedings of the Eighth Conference on Applied Climatology*. American Meteorological Society, Boston, MA, pp. 179–184.

Morid, S., Moghaddasi, M., Salavitabr, A., Delavar, M., Hosseini, S., Fathian, F., Ahmadzade, H., Sahebdel, S., Keshavarz, A., Ghaemi, H., Arshad, S., Bagheri, M. & Agha Alikhani, M. 2012 *Drought Risk Management Plan for Lake Urmia Basin: Summary Report*. Working Group on Sustainable Management of Water Resources and Agriculture, Regional Council of Lake Urmia Basin Management.

Moradi, R., Koocheki, A., Nassiri Mahallati, M. & Mansoori, H. 2013 Adaptation strategies for maize cultivation under climate change in Iran: irrigation and planting date management. *Mitigation and Adaptation Strategies for Global Change* **18**, 265–284.

Nalbantis, I. 2008 Evaluation of a hydrological drought index. *European Water* **23** (24), 67–77.

NRIDR 2005 National report of the Islamic Republic of Iran on disaster reduction. In: *World Conference on Disaster Reduction*, January, 18–22, Kobe, Hyogo, Japan.

Nyaupane, N., Raje Mote, S., Bhandari, M., Kalra, A. & Ahmad, S. 2018 Rainfall-runoff simulation using climate change based precipitation prediction in HEC-HMS model for Irwin Creek, Charlotte, North Carolina. *World Environmental and Water Resources Congress* 352–363. doi:10.1061/9780784481400.033.

O'Loughlin, F., Bruen, M. & Wagener, T. 2013 Parameter sensitivity of a watershed-scale flood forecasting model as a function of modelling time-step. *Hydrology Research* **44** (2), 334–350. doi:10.2166/nh.2012.157.

Roy, D., Begam, S., Ghosh, S. & Jana, S. 2013 Calibration and validation of HEC-HMS model for a river basin in eastern India. *ARPN Journal of Engineering and Applied Sciences* **8** (1), 40–56.

Semenov, M. A., Brooks, R. J., Barrow, E. M. & Richardson, C. W. 1998 Comparison of WGEN and LARS-WG stochastic weather generators for diverse climates. *Climate Research* **10**, 95–107. doi:10.3354/cr010095.

Tabari, H., Nikbakht, J. & Hosienzadeh Talaee, P. 2012 Hydrological drought assessment in northwestern Iran based on streamflow drought index (SDI). *Water Resources Management* **27** (1), 137–151. doi:10.1007/s11269-012-0173-3.

Taylor, K. E., Stouffer, R. J. & Meehl, G. A. 2011 An overview of CMIP5 and the experiment design. *Bulletin of the American Meteorological Society* **93**, 485–498. doi:10.1175/BAMS-D-11-00094.1.

USACE-HEC 2015 *Hydrologic Modeling System (HEC-HMS), Application Guide, Version 4.0*. US Army Corps of Engineers, Davis, CA. Hydrologic Engineering Center.

USACE-HEC 2016 *Hydrologic Modeling System HEC-HMS, User's Manual, Version 4.2*. US Army Corps of Engineers, Davis, CA. Hydrologic Engineering Center.

Vu, M. T., Vo, N. D., Gourbesville, P., Raghavan, S. V. & Liong, S.-Y. 2017 Hydro-meteorological drought assessment under climate change impact over the Vu Gia–Thu Bon river basin, Vietnam. *Hydrological Sciences Journal* **62** (10), 1654–1668. doi:10.1080/02626667.2017.1346374.

Wagener, T., van Werkhoven, K., Reed, P. & Tang, Y. 2009 Multiobjective sensitivity analysis to understand the information content in streamflow observations for distributed watershed modeling. *Water Resources Research* **45**, W02501. doi:10.1029/2008WR007347.

WAVA (Working Group of Assessing Vulnerability of Agriculture, Animal Husbandry and Fishery Sectors) 2015 *Assessing Vulnerability and Adaptation of Agricultural, Animal Husbandry and Fishery' Sectors to Climate Change: A Case of Iran*. Working Group of Assessing Vulnerability of Agriculture, Tehran, Iran.

Wilhite, D. A. & Pulwarty, R. S. 2017 Drought as Hazard: Understanding the Natural and Social Context. In: *Drought and Water Crises*, 2nd edition. CRC Press, Boca Raton, FL. doi:10.1201/b22009-2.

Yildiz, O. 2009 Assessing temporal and spatial characteristics of droughts in the Hirfanli dam basin, Turkey. *Scientific Research and Essay* **4**, 249–255.

Zheng, H., Chiew, F. H. S., Charles, S. & Podger, G. 2018 Future climate and runoff projections across South Asia from CMIP5 global climate models and hydrological modelling. *Journal of Hydrology: Regional Studies* **18**, 92–109. doi:10.1016/j.ejrh.2018.06.004.

First received 30 June 2020; accepted in revised form 2 December 2020. Available online 16 December 2020